Spacer Intercalated Disassembly and Photodynamic Activity of Zinc Phthalocyanine Inside Nanochannels of Mesoporous Silica Nanoparticles

ARTICLE *in* ACS APPLIED MATERIALS & INTERFACES · DECEMBER 2013

Impact Factor: 6.72 · DOI: 10.1021/am404578h · Source: PubMed

3 AUTHORS, INCLUDING:

Xing Ma
Max Planck Institute for Intelligent Systems, S…
42 PUBLICATIONS **871** CITATIONS
SEE PROFILE

Sivaramapanicker Sreejith
Nanyang Technological University
41 PUBLICATIONS **1,055** CITATIONS
SEE PROFILE

ACS APPLIED MATERIALS & INTERFACES

Research Article

www.acsami.org

Spacer Intercalated Disassembly and Photodynamic Activity of Zinc Phthalocyanine Inside Nanochannels of Mesoporous Silica Nanoparticles

Xing Ma,[†,§] Sivaramapanicker Sreejith,[†,§] and Yanli Zhao*[,†,‡]

[†]Division of Chemistry and Biological Chemistry, School of Physical and Mathematical Sciences, Nanyang Technological University, 21 Nanyang Link, 637371 Singapore

[‡]School of Materials Science and Engineering, Nanyang Technological University, 50 Nanyang Avenue, 639798 Singapore

Supporting Information

ABSTRACT: Hydrophobic photosensitizer zinc(II) phthalocyanine (ZnPc) was loaded into adamantane (Ad) modified nanochannels of mesoporous silica nanoparticles (MSNPs). The Ad units on the surface of MSNPs were complexed with amino-substituted β-cyclodextrin to enhance the solubility of the hybrid in aqueous solution. The amino groups on β-cyclodextrin also provide functional sites for further conjugation with targeting ligands toward targeted cancer therapy. Since the intercalation of the Ad spacer isolates loaded ZnPc and prevents its aggregation inside MSNPs, ZnPc exhibits its monomeric characteristics to effectively generate cytotoxic singlet oxygen ($^1O_2$) upon light irradiation (675 nm) in aqueous conditions, leading to efficient photodynamic activity for successful cancer treatment in vitro. Current research presents a convenient approach to maintain the monomeric state of hydrophobic photosensitizer ZnPc by rationally utilizing multifunctional MSNPs as the carriers. The novel hybrid with targeting capability achieves active photodynamic property of monomeric ZnPc in aqueous solution under light irradiation, which may find its way for practical photodynamic therapy in the future.

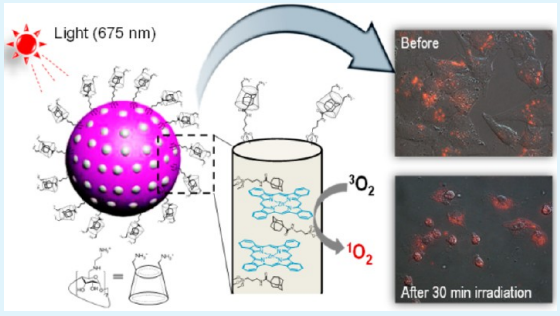

KEYWORDS: *cancer cell death, mesoporous silica nanoparticles, photodynamic therapy, singlet oxygen, targeted therapy, zinc(II) phthalocyanine*

1. INTRODUCTION

Photodynamic therapy (PDT) is a relatively inexpensive and noninvasive method for cancer treatment.[1−6] It has been proved to be an ideal approach for the treatment of skin cancer[7] and also found effective for the treatment of early lung cancer,[8] bladder cancer,[9] as well as head and neck cancers.[10] In PDT-based treatments, tumor cells are destroyed by irradiating light on photosensitizers to induce the production of reactive oxygen species, primarily cytotoxic singlet oxygen ($^1O_2$), in a localized area. Thus, an ideal photosensitizer should possess high absorption coefficient, high quantum yield of the triplet state, and low dark cytotoxicity in physiological conditions. Low solubility of most photosensitizers in aqueous solution, however, limits their biological applications. Although the carriers such as polymers,[11] liposomes,[12,13] and metal nanoparticles[14−17] have been developed to enhance the solubility and targeted therapy of photosensitizers, the quest for a versatile and safe nanocarrier is still challenging.

Mesoporous silica nanoparticles (MSNPs) have attracted a great deal of interest for their uses as the drug delivery platforms on account of their versatility and low cytotoxic features within a normal dosage range employed in biological systems.[18,19] Moreover, the US food and drug administration (FDA) considers silica nanoparticles to be in the "generally recognized safe" category.[20] As promising drug carriers, MSNPs with remarkable advantages, such as large surface area, uniform mesopores, and easy chemical functionalization, open up new pathways for multiple applications. Hence, significant research effort has centered on constructing multifunctional MSNPs[21−23] and their hybrids towards cancer biolabeling[24−27] and therapeutics.[28−31] In general, the internalization of photosensitizer-loaded nanoparticles demands the optimization of few parameters including the maximum cell targeting, the maximum photosensitizer loading without aggregation, the maximum photodynamic toxicity, and the minimum dark cytotoxicity. Among these parameters, the tumor targeting can be achieved either by passive targeting owing to the enhanced permeability and retention (EPR) observed in tumor sites[32,33] or by introducing targeting ligands onto the nanoparticle carriers to hunt down specific tumor cells.

In our present study, we selected zinc(II) phthalocyanine (ZnPc), a second-generation photosensitizer, for the investigations. ZnPc normally suffers severe aggregation, thereby losing its singlet oxygen ($^1O_2$) generation efficiency in aqueous

Received: July 27, 2013
Accepted: December 6, 2013
Published: December 6, 2013

Scheme 1. Schematic Illustration for the Preparation of ZnPc-Loaded MSNP-Ad and Its Complex with CD-2NH$_2$ (MSNP-Ad +ZnPc+CD-2NH$_2$) for Photodynamic Singlet Oxygen Generation[a]

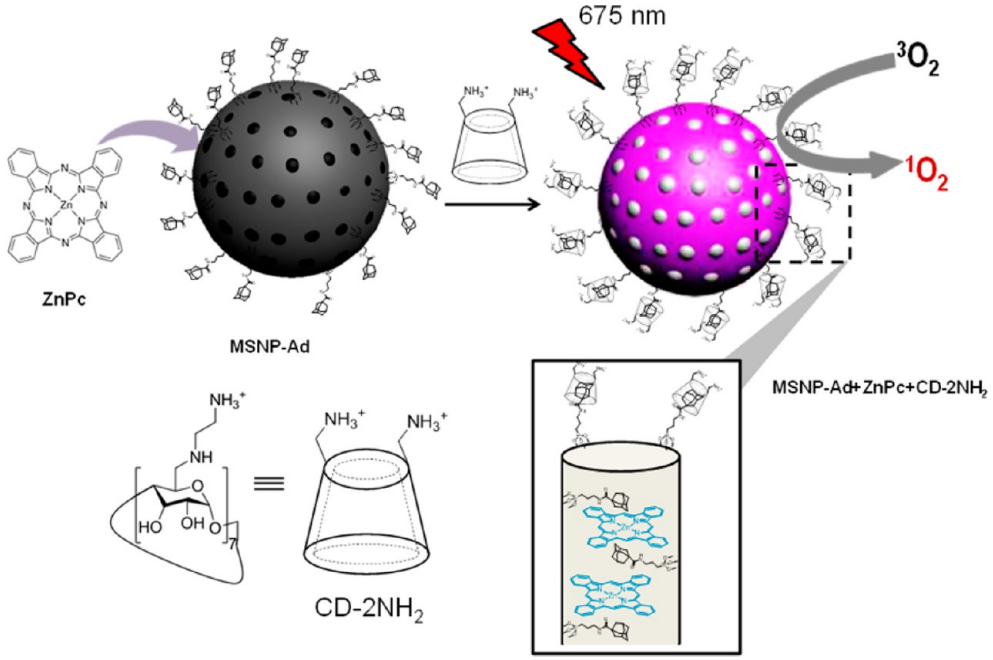

[a]Enlarged area represents a nanochannel modified with the Ad spacer that prevents ZnPc from the aggregation.

environments. The easy aggregation significantly limits its application potential in physiological environments. Thus, intensive work has been carried out forward, developing alternative strategies to effectively use ZnPc for PDT.[34,35] For example, a recent paper reported the development of gold nanoparticle/ZnPc conjugates for addressing the issue.[36]

Herein, we describe a hitherto unreported method for controlling the self-assembly of ZnPc inside nanochannels of MSNPs (Scheme 1). We anticipated that hydrophobic spacers, such as adamantane (Ad), functionalized inside the mesopores of MSNPs could intervene between ZnPc molecules, instantly preventing loaded ZnPc from the aggregation. On account of the space confinement of Ad-functionalized nanochannels, the loaded ZnPc could be completely separated, presenting its monomeric state inside MSNPs. Such strategy led to highly efficient $^1O_2$ generation from ZnPc-loaded MSNPs inside a biological environment upon light irradiation (675 nm) with a low light power output. Concurrently, the modified Ad units on the surface of MSNPs complexed with amino-substituted β-cyclodextrin (CD-2NH$_2$) could enhance the dispersibility of the hybrid in aqueous conditions, facilitating the nanoparticle hybrid to be endocytosed by cancer cells for improving PDT-based cancer therapy efficiency. Moreover, the conjugation of a cancer-targeting ligand, folic acid (FA), with the amino groups of CD-2NH$_2$ on the nanoparticle surface provides the feasibility of targeted cancer therapy based on the PDT process.

2. EXPERIMENTAL SECTION

Materials. Adamantane-1-carboxylic acid, 3-aminopropyltriethoxysilane (APTES), annexin V and propidium iodide apoptosis/cell death assay kits, cetyltrimethylammonoium bromide (CTAB, 90%), dicyclohexylcarbodiimide (DCC), dimethylformamide (DMF, 99%), dimethyl sulfoxide (DMSO), 3-(4,5-dimethylthiazol-2-yl)-2,5-diphenyltetrazolium bromide (MTT), Dulbecco's modified eagle's medium (DMEM), 1-ethyl-3-(3-dimethylaminopropyl)carbodiimide (EDC), fetal bovine serum (FBS), fluorescein isothiocyanate (FITC), hydrochloride (HCl, assay 37%), *N*-hydroxylsuccinimide (NHS), phosphate-buffered saline (PBS, pH 7.2), buffer, and tetraethylorthosilicate (TEOS, 99%) were purchased commercially.

Instruments. Field emission scanning electron microscopy (FE-SEM) and transmission electron microscopy (TEM) images were captured by FESEM 6340 at 5 kV and JEOL 2010 TEM at 200 kV, respectively. An X-ray diffraction pattern was collected by Shimadzu Powder XRD from $2\theta = 1.6$ to 8. Zeta potential value and hydrodynamic size were measured by Mavern Nanosizer, and each sample was measured three times for statistical analysis. Surface area and pore size distribution of the nanoparticles were characterized by ASAP-2020 Micromeritics. Fourier-transformed infrared (FT-IR) spectra were measured through a Fourier-transformed infrared spectrometer. UV–vis absorption was measured by an UV–vis 2501 spectrometer. Fluorescence emission spectra were collected by an RF 5301 spectrofluorimeter. Thermogravimetric analysis (TGA) was carried out by a Q500 thermogravimetric analyzer. A microplate reader (infinite 200 PRO, Tecan) was used for the MTT assay. Fluorescence images were taken by a confocal fluorescence microscope (Nikon, Eclipse TE2000-E, 60 × oil objective). Flow cytometry data were collected by a BD FACS Calibur Flow Cytometer.

MSNPs, MSNP-NH$_2$, and MSNP(FITC)-NH$_2$. MSNPs were prepared according to a previous report with some modifications.[37] In a typical synthesis, CTAB (500 mg) was dissolved in distilled H_2O (250 mL). NaOH aqueous solution (1.75 mL, 2 M) was added into the above solution. The mixture solution was heated to 80 °C under vigorous stirring. When the temperature was stabilized, TEOS (2.5 mL) was slowly added into the mixture solution. For bare MSNPs, the mixed solution was kept stirring for 2 h to form white precipitates.

Amino group functionalized silica nanoparticles (MSNP-NH$_2$) were prepared by a co-condensation method in basic solution to obtain a uniform distribution of the functional groups both inside the mesopores and on the nanoparticle surface.[25] Specifically, after addition of TEOS in the previous step for 15 min, APTES (0.5 mL) was added dropwise. The mixture solution was stirred at 80 °C for another 2 h. Then, the formed nanoparticles were collected by centrifugation at 8000 rpm for 10 min and washed with MeOH and distilled H_2O. Surfactant was removed by suspending the obtained nanoparticles in MeOH (150 mL) containing condensed HCl (9 mL, 37%) and then refluxing at 80 °C for 24 h.

The obtained nanoparticles were collected by centrifugation and washed thoroughly with MeOH and distilled H_2O. The nanoparticles were dried in vacuo at 50 °C for 24 h.

As for FITC-labeled nanoparticles (MSNP(FITC)-NH_2),[38] FITC (1.3 mg) was dissolved in absolute ethanol (1.5 mL) containing APTES (3μL), and the mixture solution was gently stirred for 2 h in the dark before adding into the CTAB-TEOS solution as described above.

Solid SiO_2−NH_2. The solid SiO_2 nanoparticles were first prepared by using the modified Stöber method.[39] Typically, EtOH (71.4 mL), distilled water (10 mL), and ammonium aqueous solution (25−28%, 2 mL) were mixed under stirring. After the mixture solution was heated to 30 °C, TEOS (2.5 mL) was added to the mixture solution. The reaction mixture was stirred at 30 °C for 6 h. The formed solid silica nanoparticles were collected by centrifugation and washed with distilled H_2O and EtOH thoroughly. Then, solid SiO_2 nanoparticles (100 mg) were suspended in absolute EtOH containing APTES (20 μL), and the mixture was stirred for 48 h to afford amino group functionalized solid silica nanoparticles (solid SiO_2−NH_2). The formed nanoparticles were collected by centrifugation and washed extensively by EtOH.

MSNP-Ad, MSNP(FITC)-Ad, and Solid SiO_2-Ad. Adamantane-1-carboxylic acid (225 mg) was dissolved in DMF (10 mL) containing DCC (645 mg) and NHS (360 mg). After the mixture solution was stirred for 2 h, a DMF (5 mL) solution containing fully suspended MSNP-NH_2, MSNP(FITC)-NH_2, or solid SiO_2−NH_2 (100 mg) was added. After reacting for 24 h, MSNP-Ad, MSNP(FITC)-Ad, or solid SiO_2-Ad nanoparticles were collected by centrifugation and washed with DMF, MeOH, and distilled H_2O extensively.

CD-2NH_2. Ethylenediamine-modified β-cyclodextrin derivative (CD-2NH_2) was prepared according to a previous report.[37] Seven ethylenediamine groups were covalently linked at the primary side of the β-cyclodextrin ring.

MSNP-Ad+ZnPc+CD-2NH_2 and MSNP(FITC)-Ad+ZnPc+CD-2NH_2. MSNP-Ad (1 mg) was suspended in DMF solution (1 mL) containing ZnPc (0.1 mg mL^{-1}). After stirring for 24 h, ZnPc-loaded MSNP-Ad, denoted as MSNP-Ad+ZnPc, was collected by centrifugation at 13 000 rpm for 3 min. After washing with PBS, CD-2NH_2 (1 mg mL^{-1}) was added into the nanoparticle suspension. The reaction mixture was stirred for 12 h to complete the complex formation, which was then centrifuged at 8000 rpm followed by washing with PBS to obtain ZnPc-loaded and CD-2NH_2-capped MSNP-Ad, noted as MSNP-Ad+ZnPc+CD-2NH_2. FITC-labeled nanoparticles, i.e., MSNP(FITC)-Ad+ZnPc+CD-2NH_2, were also prepared using MSNP-(FITC)-Ad under a similar method.

MSNP-Ad+ZnPc+CD-FA and MSNP(FITC)-Ad+ZnPc+CD-FA. FA was conjugated through amide bond formation between the carboxylic acid group on FA and the amino group on CD-2NH_2. First, activated FA was prepared. FA (200 mg) was mixed with DCC (120 mg) and NHS (120 mg) in DMSO (10 mL). After stirring for 24 h, the mixture solution was centrifuged, and the supernatant containing activated FA was collected and stored at 4 °C for future use. Then, MSNP-Ad+ZnPc+CD-2NH_2 (1 mg) was suspended in PBS (1 mL, pH 7.2). An aqueous solution (1 mL) containing activated FA (50 μg) was added into the suspension. The mixture solution was stirred for 24 h. The formed MSNP-Ad+ZnPc+CD-FA was collected by centrifugation and washed with PBS three times. FITC-labeled nanoparticles, i.e., MSNP(FITC)-Ad+ZnPc+CD-FA, were also prepared using MSNP(FITC)-Ad+ZnPc+CD-2NH_2 under a similar method.

Determination of ZnPc Loading Capacity. MSNPs, MSNP-Ad, or solid SiO_2-Ad (1 mg) was suspended in DMF solution (1 mL) containing ZnPc (0.1 mg mL^{-1}). After stirring for 24 h, ZnPc-loaded nanoparticles were collected by centrifugation at 13 000 rpm for 3 min. After washing with PBS twice, the nanoparticles were suspended in DMF, and the loaded ZnPc was extracted by thorough sonication for 30 min. Then, the suspension was centrifuged at 13 000 rpm for 3 min, and the supernatant was collected. The extraction process was performed repeatedly until a white pellet was obtained after the centrifugation. The ZnPc amount in all the collected supernatants was quantified by the UV−vis absorption intensity at 675 nm.

Cell Culture. HeLa cells were cultured in DMEM containing 10% FBS and nonessential amino acids (0.1 mM). The culture was maintained at 37 °C in a humidified atmosphere containing 5% CO_2.

MTT Cytotoxicity Assay. A photodynamic cytotoxicity effect was evaluated by the MTT assay. HeLa cells or HEK293 cells were seeded into a 96-well plate at a density of 1×10^4 cells/well in complete DMEM medium and grown for 24 h. Then, MSNP-Ad+ZnPc+CD-2NH_2 or MSNP-Ad+ZnPc+CD-FA was added into each well at different concentrations. After exposure to the nanoparticles for 24 h, the medium in each well was removed, and the cells were washed by PBS twice to remove free nanoparticles in the medium. Fresh complete DMEM medium (100 μL) was added into each well. After 4 h incubation, the cells were exposed to 675 nm light for a certain period of time followed by further incubation for 24 h. The MTT assay was then conducted by replacing the medium in each well with a new medium containing MTT (100 μL, 0.5 mg mL^{-1}). After incubation for 4 h, the medium was removed, and DMSO (100 μL) was added into each well. The plate was gently shaken for 15 min, and absorbance intensity at 565 nm was recorded using a microplate reader. The relative cell viability related to control wells that were only treated with medium was calculated by $[A]_{test}/[A]_{control}$, where $[A]_{test}$ and $[A]_{control}$ are the average absorbance of the test and control samples, respectively.

Fluorescence Microscopy Images. HeLa cells were seeded in 35 mm plastic-bot-tomed μ-dishes and grown in complete DMEM medium for 24 h. Then, HeLa cells were treated with MSNP(FITC)-Ad +ZnPc+CD-2NH_2 (20 μg mL^{-1}). After 24 h incubation, the medium was removed, and the cells were washed three times with PBS buffer (pH 7.2) and fixed with 4.0% formaldehyde at room temperature for 15 min. After removing 4.0% formaldehyde, the cells were washed with PBS buffer (pH 7.2) three times before capturing the fluorescence images using a fluorescence microscope. For apoptosis and cell death assay, after HeLa cells were treated with MSNP-Ad+ZnPc+CD-2NH_2 (20 μg mL^{-1}) for 24 h, the medium was removed, and the cells were washed by PBS buffer thrice. Then, a new medium was added into the cells. After 4 h incubation, the cells were exposed to 675 nm light irradiation (2.5 mW cm^{-2}) for 20 min. After another 24 h incubation, the cells were washed by PBS and then stained by the apoptosis kit (both annexin V and propidium iodide) according to the instruction of the kit. The cell nucleus was stained by 4′,6-diamidino-2-phenylindole (DAPI). Finally, the cells were observed under fluorescence microscopy.

Bio-TEM Analysis. After HeLa cells were treated with MSNP-Ad +ZnPc+CD-2NH_2 (20 μg mL^{-1}) for 24 h, the medium was removed, and the cells were washed repeatedly. Then, a new medium was added to the cells. After 4 h incubation, the cells were exposed to 675 nm light irradiation (2.5 mW cm^{-2}) for 20 min. After another 12 h or 24 h incubation, the cells were washed again with PBS followed by fixing with 2.5% glutaraldehyde at 4 °C overnight. Hereafter, cells were washed with 0.1% phosphate buffer and post-fixed with 1% osmium tetroxide at room temperature for 1 h. Fixed cell pellets were further washed, and dehydration was performed in increasing grades of ethanol (25%−100%) and pure acetone. Infiltration in SPI-Pon-Araldite (SPI, USA) resin was carried out at room temperature overnight followed by pure resin embedding at 60 °C for 72 h. The obtained blocks were sectioned by an ultramicrotome, and ultrathin sections were stained with lead citrate. The grids were observed by TEM.

Flow Cytometry Experiments. HeLa cells or HEK293 cells were seeded in 6-well plates and grown in complete DMEM medium for 24 h. The cells were treated with MSNP(FITC)-Ad+ZnPc (20 μg mL^{-1}), MSNP(FITC)-Ad+ZnPc+CD-2NH_2 (20 μg mL^{-1}), and MSNP(FITC)-Ad+ZnPc+CD-FA (20 μg mL^{-1}), respectively. After 24 h incubation, the cells were washed by PBS three times and harvested by trypsin treatment. Then, the cells were centrifuged and washed by PBS twice before conducting flow cytometry detection.

For the apoptosis and cell death assay, after HeLa cells were treated with MSNP-Ad+ZnPc+CD-2NH_2 (20 μg mL^{-1}) for 24 h, the medium was removed, and the cells were washed thrice by PBS buffer. Then, a new medium was added to the cells. After 4 h incubation, the cells were exposed to 675 nm light irradiation (2.5 mW cm^{-2}) for 20 min. After another 24 h incubation, the cells were collected by trypsin and washed with PBS buffer through centrifugation. The cells were stained by the apoptosis/cell death assay kit according to the product instructions, and then flow cytometry analysis was performed.

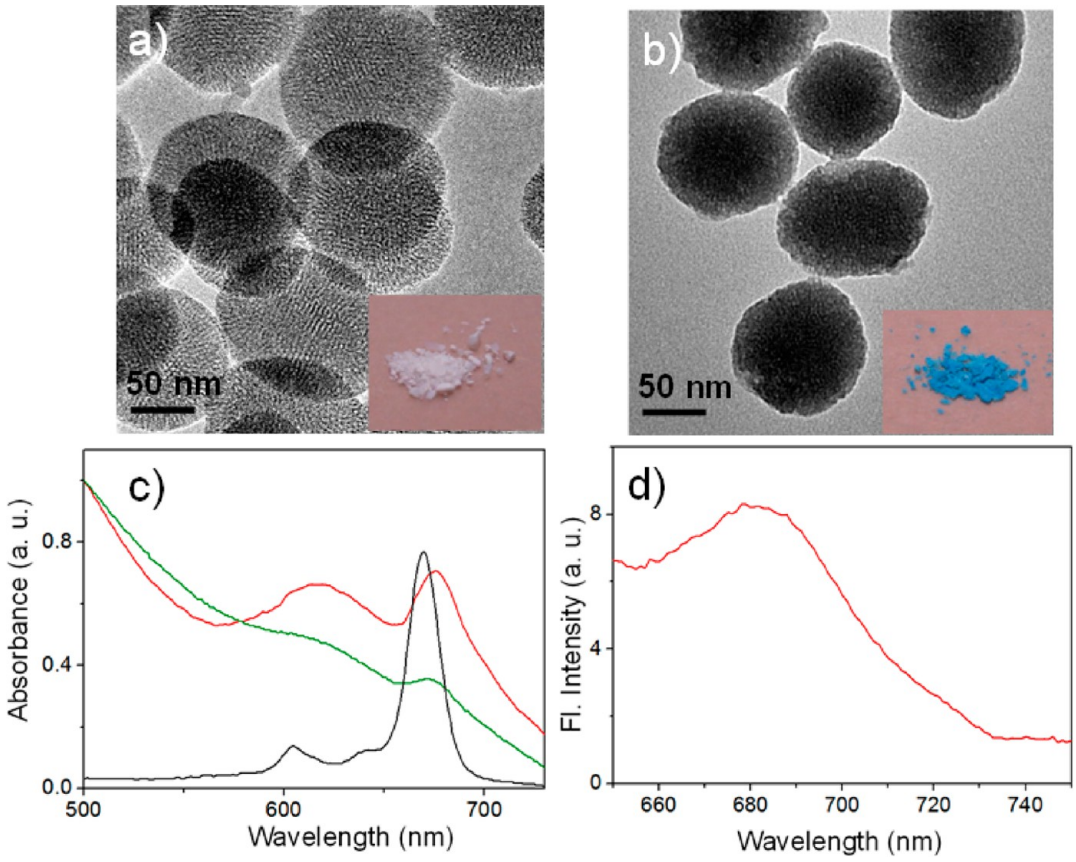

Figure 1. TEM images of (a) MSNP-Ad and (b) MSNP-Ad+ZnPc+CD-2NH_2. Insets are the photographs of the corresponding nanoparticles under visible light. (c) UV−vis absorption spectra of MSNP-Ad+ZnPc (green curve) and MSNP-Ad+ZnPc+CD-2NH_2 (red curve) in PBS buffer (pH 7.2), as well as of ZnPc alone in DMF (black curve, 4.8×10^{-7} M). (d) Emission spectrum of MSNP-Ad+ZnPc+CD-2NH_2 in PBS buffer (pH 7.2).

For the fluorescence microscopy observations, after the treatments with the nanoparticle hybrids and light irradiation, the cells were directly stained by the apoptosis/cell death assay kit according to the product instructions and then observed by fluorescence microscopy.

3. RESULTS AND DISCUSSION

In this work, we first synthesized MSNP-NH_2 via a co-condensation method[37] and bare MSNPs without any functional groups as a control. Then, Ad was covalently conjugated with amino groups of MSNP-NH_2, and it was coupled onto both the nanoparticle surface and nanochannels to form MSNP-Ad (Scheme 2). Hydrophobic ZnPc was loaded into the nanochannels of MSNP-Ad in DMF, yielding MSNP-Ad+ZnPc. The MSNP-Ad+ZnPc+CD-2NH_2 hybrid was prepared by making use of strong inclusion complexation between Ad and β-cyclodextrin. Thus, the complex formation between the Ad unit on the nanoparticle surface of MSNP-Ad+ZnPc and CD-2NH_2 was carried out in aqueous solution (Scheme 1). In addition to enhanced dispersion of the hybrid in aqueous environments on account of the CD-2NH_2 complexation, the loaded ZnPc presents characteristic properties in its monomeric state. The CD-2NH_2 ring could also block ZnPc inside the nanoparticles without any leakage. The hybrid shows excellent cell permeability and efficient generation of $^1O_2$ upon irradiation with monochromatic light at 675 nm. Solid SiO_2−NH_2 and solid SiO_2-Ad were also prepared as the control groups.

Figure 1a shows a TEM image of MSNP-Ad in a diameter range of 100−120 nm with clear mesoporous structures. Inset is the photograph of MSNP-Ad under visible light, showing colorless powder. After the mesopores were occupied by ZnPc in MSNP-Ad+ZnPc+CD-2NH_2 (Figure 1b), they cannot be clearly observed by TEM when compared to that of MSNP-Ad. The inset of Figure 1b shows the photograph of MSNP-Ad+ZnPc +CD-2NH_2 under visible light, giving blue color. While preparing ZnPc-loaded MSNP-Ad to keep ZnPc mostly in its monomeric state inside the mesopores, a solution of ZnPc with a concentration of 0.1 mg mL^{-1} was used. The dispersion of ZnPc in MSNP-Ad was monitored by the UV−vis spectrum. ZnPc in DMF has a characteristic absorption maximum at 669 nm (black curve in Figure 1c). ZnPc loaded inside the mesopores of MSNP-Ad in PBS buffer exhibits a slight bathochromic shift of the absorption maximum to 672 nm (green curve in Figure 1c). The Ad spacer could prevent the aggregation of ZnPc inside the mesopores to a great extent. The amount of ZnPc loaded in MSNP-Ad was determined spectrophotometrically to be 0.6 wt %, by sonicating ZnPc-loaded MSNP-Ad in DMF thoroughly to extract out all ZnPc molecules. Then, all the extracted ZnPc in DMF solution was quantified by its UV−vis absorbance intensity. As compared with MSNP-Ad+ZnPc, MSNP-Ad+ZnPc+CD-2NH_2 in PBS buffer exhibits a further bathochromic shift of the absorption maximum to 675 nm (red curve in Figure 1c, $\Delta\lambda$ = 5 nm), which is a characteristic monomer signature of ZnPc inside the mesopores. The emission spectrum was also recorded in PBS buffer at pH 7.2. When excited at 610 nm, the MSNP-Ad+ZnPc+CD-2NH_2 hybrid (0.5 mg mL^{-1}) shows the emission maximum of ZnPc at 680 nm (Figure 1d) with a fluorescence quantum yield (Φ_F) of 0.11 relative to ZnPc in DMF (Φ_F = 0.28).[40,41] The absorption

Scheme 2. Schematic Representation for the Preparation of MSNP-Ad

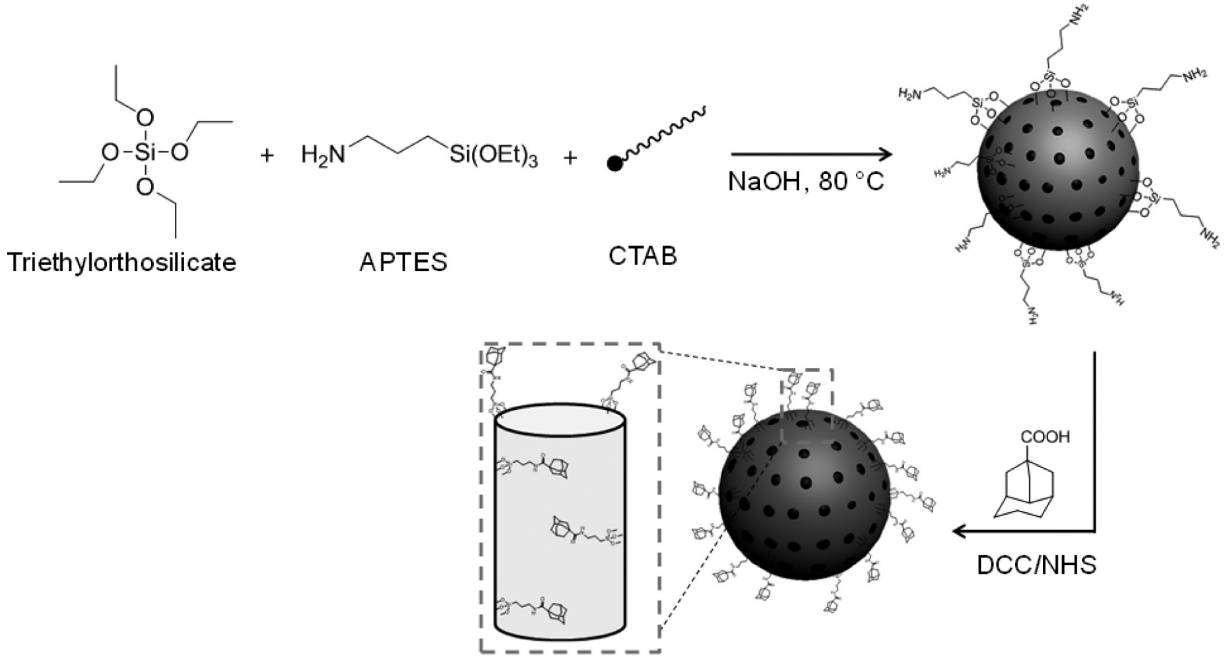

and fluorescence properties provide clear evidence for the monomeric existence of ZnPc inside the nanochannels with the Ad spacers.

Powder X-ray diffraction pattern of MSNP-Ad demonstrates hexagonal packing of MCM-41 type mesoporous structure with a clear (100) peak at 2θ = 2.14 (Figure S1 in the Supporting Information (SI)). The nanoparticle size of MSNP-Ad was estimated to be about 100−120 nm in diameter, which is basically consistent with the size distribution determined by TEM (Figure 1a) and FE-SEM (Figure S2 in the SI). Surface area and porous nature of MSNP-NH_2, MSNP-Ad, and MSNP-Ad +ZnPc were characterized by N_2 adsorption/desorption measurements. Typical type-IV isotherms (Figure S3a in the SI), indicative of mesoporous structure, were observed for both MSNP-NH_2 and MSNP-Ad, giving a BET (Brunauer−Emmett−Teller) surface area of 1116.63 $m^2\ g^{-1}$ for MSNP-NH_2 and 852.58 $m^2\ g^{-1}$ for MSNP-Ad (Table S1 in the SI). The BET experiments indicate that the introduction of the Ad unit did not obviously block the mesopores. The decreases in the BJH (Barrett−Joyner−Halenda) pore size from 2.81 to 2.52 nm and the pore volume from 0.98 to 0.83 $cm^3\ g^{-1}$ after the introduction of the Ad unit to MSNP-NH_2 proved successful internal modification of the nanochannels with the Ad spacer (Figure S3b and Table S1 in the SI). After loading ZnPc into the mesopores of MSNP-Ad, the surface area, pore size, and pore volume of MSNP-Ad+ZnPc were significantly dropped.

The functionalization process was also traced by FT-IR spectra (Figure S4 in the SI). After the Ad modification, a new peak at 1560 cm^{-1} corresponding to N−H bending from the amide bond was observed from the FT-IR spectrum of MSNP-Ad. In addition, the amount of the functional groups in the nanoparticles could be roughly estimated from the TGA results (Figure S5 in the SI). The extra 6 wt % (i.e., 1.15 mmol g^{-1}) weight loss in MSNP-NH_2 (black curve in Figure S5, SI) as compared to MSNPs (blue curve in Figure S5, SI) was contributed to amino functional groups (−NH_2), and further 7 wt % (i.e., 0.514 mmol g^{-1}) weight loss in MSNP-Ad (red curve in Figure S5, SI) as compared to MSNP-NH_2 was attributed to the introduction of the Ad spacer.

Furthermore, zeta-potential measurements indicate that, after the Ad functionalization, the nanoparticle surface charge decreased from 24 to 6.7 mV owing to the replacement of amino groups with the Ad units. A similar charge decrease was found after converting solid SiO_2−NH_2 to solid SiO_2-Ad. The complex formation between the Ad unit and CD-2NH_2 in MSNP-Ad+ZnPc+CD-2NH_2 was further evidenced from enhanced surface charge to 23.3 mV (Table S2 in the SI). Dynamic light scattering (DLS) measurements reveal that the DLS size of the nanoparticles decreased from MSNP-Ad+ZnPc to MSNP-Ad+ZnPc+CD-2NH_2 (Table S2 in the SI), indicating that the introduction of CD-2NH_2 enhances the dispersibility of MSNP-Ad+ZnPc+CD-2NH_2 in aqueous solution.

To further study the role of the Ad spacer in isolating ZnPc in the nanoparticles, ZnPc was loaded into MSNPs without the Ad modification, giving MSNP+ZnPc. Although a similar loading capacity between MSNPs (0.5 wt %) and MSNP-Ad (0.6 wt %) was found (Table S3 in the SI), no characteristic absorption peak around 675 nm corresponding to monomeric ZnPc was observed for MSNP+ZnPc (Figure S6 in the SI). In addition, we also tried to attach ZnPc onto solid SiO_2-Ad nanoparticles with a diameter of about 100 nm. The solid SiO_2-Ad nanoparticles were characterized by TEM and FT-IR spectra (Figures S7 and S8 in the SI). After carrying out the same loading procedure on solid SiO_2-Ad, much lower loading capacity (<0.1 wt %) and no absorption peak corresponding to ZnPc were observed (Table S3 and Figure S6 in the SI). These observations clearly demonstrate that ZnPc was indeed loaded into the nanochannels of MSNP-Ad, and the Ad units modified on the nanochannels could effectively serve as the spacers to prevent loaded ZnPc from the aggregation.

We then investigated photoinduced $^1O_2$ generation capability of the MSNP-Ad+ZnPc+CD-2NH_2 hybrid through an indirect chemical method using ADMA (9,10-anthracenediyl-bis-(methylene)dimalonic acid) as the $^1O_2$ trap agent. ADMA reacts with $^1O_2$ to produce corresponding endoperoxide that can be followed by absorption changes of ADMA.[14,42] ADMA

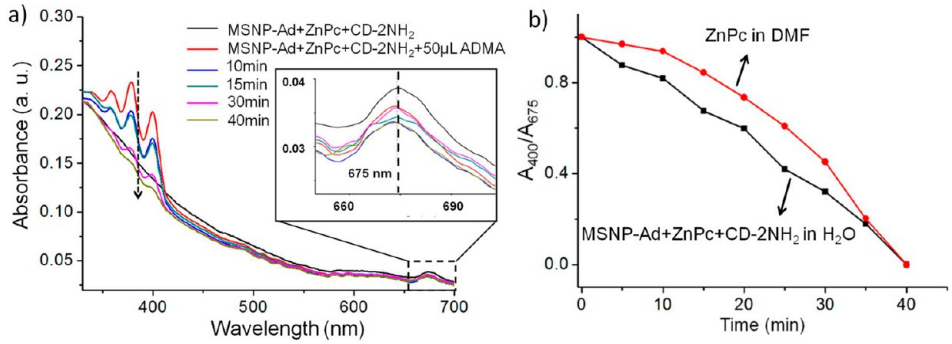

Figure 2. (a) UV−vis absorption changes (between 340 and 420 nm) showing a decrease in the absorption of ADMA upon irradiating MSNP-Ad+ZnPc +CD-$2NH_2$ with 675 nm light for 40 min. Inset shows an enlarged area corresponding to the absorption changes of monomeric ZnPc inside MSNP-Ad +ZnPc+CD-$2NH_2$. (b) A ratiometric plot showing the $^1O_2$ generation performance of ZnPc in DMF (red curve) and MSNP-Ad+ZnPc+CD-$2NH_2$ in water by comparing the ratio of absorption intensity changes between ADMA at 400 nm (A_{400}) and ZnPc at 675 nm (A_{675}) against irradiation time.

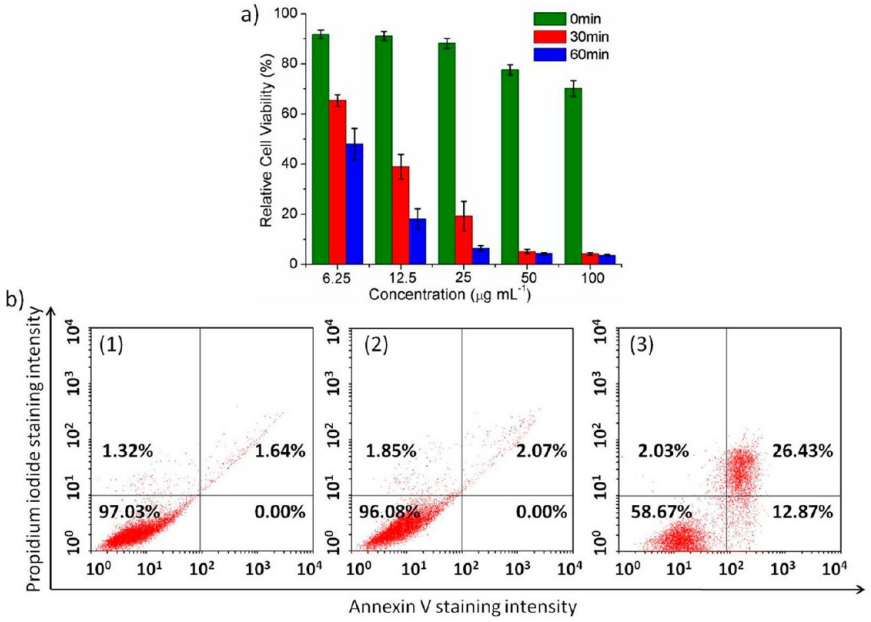

Figure 3. (a) Photodynamic cytotoxicity of HeLa cells determined by MTT cell viability assay. The cells were incubated with MSNP-Ad+ZnPc+CD-$2NH_2$ for 24 h followed by irradiation at 675 nm light for 30 min (red bars) and 60 min (blue bars). Another set of cells was incubated with MSNP-Ad +ZnPc+CD-$2NH_2$ in the dark as a control (green bars). The concentrations refer to the amounts of MSNP-Ad used. (b) Apoptosis/cell death assay of HeLa cells determined by flow cytometry. HeLa cells without any treatment were used as a control (b1). HeLa cells were incubated with MSNP-Ad +ZnPc+CD-$2NH_2$ (20 μg mL^{-1}) for 24 h followed by incubation in the dark (b2) or irradiation under 675 nm light for 20 min (b3).

(6×10^{-5} M) was added into PBS buffer (pH 7.2) containing MSNP-Ad+ZnPc+CD-$2NH_2$ (0.5 mg mL^{-1}) under stirring. A typical absorption spectrum of the mixture shows two characteristic regions (Figure 2a); i.e., absorption corresponding to ADMA is at 350−415 nm, and absorption for ZnPc is from 650 to 690 nm. The absorption of ADMA decreased continuously, when the mixture was irradiated under 675 nm light for 40 min. It should be noted that the power of the light source used in the study was 2.5 mW cm^{-2}, which was much lower than that employed in previous reports using ZnPc for PDT-based cancer therapy.[43−45] Photobleaching of ADMA confirmed efficient generation of $^1O_2$ from ZnPc inside Ad-modified mesopores. A ratiometric plot by comparing the absorption intensity changes between ZnPc in DMF and MSNP-Ad+ZnPc+CD-$2NH_2$ in water against irradiation time clearly reveals the $^1O_2$ generation capability of ZnPc inside the mesopores of MSNP-Ad. Therefore, effective $^1O_2$ generation of MSNP-Ad+ZnPc+CD-$2NH_2$ in aqueous conditions provides a proof-of-concept for our strategy of preventing ZnPc from its aggregation inside the nanochannels of MSNP-Ad.

To prove that the introduction of CD-$2NH_2$ could enhance cellular internalization of the MSNP-Ad+ZnPc+CD-$2NH_2$ hybrid, we carried out parallel in vitro experiments using FITC-labeled nanoparticles. MSNP(FITC)-Ad+ZnPc and its CD-$2NH_2$ complex, i.e., MSNP(FITC)-Ad+ZnPc+CD-$2NH_2$, were prepared accordingly for detailed investigations. The two hybrids containing both ZnPc and FITC dyes with different excitation wavelengths can be easily traced in vitro from green (FITC) and red (ZnPc) excitation channels. We incubated HeLa cells with the two hybrids, respectively. Figure S9 in the SI shows the images of HeLa cell lines incubated with either MSNP(FITC)-Ad+ZnPc (row 1 in Figure S9a, SI) or MSNP(FITC)-Ad+ZnPc+CD-$2NH_2$ (row 2 in Figure S9a, SI) after 24 h, and obvious intracellular fluorescence indicates much better cellular internalization capability of MSNP(FITC)-Ad +ZnPc+CD-$2NH_2$. Intracellular localization and accumulation

experiments conducted using the two hybrids under the same conditions provide unambiguous evidence for enhanced internalization of MSNP(FITC)-Ad+ZnPc+CD-2NH_2. The flow cytometry analysis (Figure S9b in the SI) presents further proof for the enhanced uptake of MSNP(FITC)-Ad+ZnPc+CD-2NH_2 since its intracellular fluorescence intensity is more significant as compared with that of MSNP(FITC)-Ad+ZnPc without the CD-2NH_2 capping. Thus, the enhancement in cellular uptake via the CD-2NH_2 complexation endows high nanoparticle concentration inside the cell lines, which is beneficial to achieve apparently high photodynamic toxicity under light irradiation. Moreover, we investigated the release profile of ZnPc from MSNP-Ad+ZnPc +CD-2NH_2 in PBS buffer at pH 7.2, and no ZnPc release was observed after three days (Figure S10 in the SI). The observation demonstrates a good capping capability of the CD-2NH_2 ring on the nanoparticle surface, blocking ZnPc inside the mesopores from the leakage.[46]

To examine the PDT efficiency of MSNP-Ad+ZnPc+CD-2NH_2, the MTT cell viability assay on HeLa cancer cell lines was performed. The in vitro photodynamic toxicity was investigated by using a monochromatic light with a low power of 2.5 mW cm^{-2}. HeLa cells were first incubated with MSNP-Ad+ZnPc+CD-2NH_2 at a series of concentrations for 24 h and then washed with PBS buffer twice to remove residual nanoparticles that were not consumed by cells. Light irradiation experiments were carried out using an in-house developed experimental setup (Figure S11 in the SI). After 48 h incubation followed by irradiation, the cell viability was examined by MTT. Control experiments were also conducted by keeping the samples in the dark. Figure 3a shows the results of the MTT viability assay using different amounts of MSNP-Ad +ZnPc+CD-2NH_2. Even at the maximum possible concentration in the dark, relatively low cytotoxicity (green bars) was observed. Higher photodynamic cytotoxicity of the hybrid was observed after irradiating the cells for 60 min than that for 30 min. For the case of 30 min light irradiation, the half maximal inhibitory concentration (IC_{50}) was found to be only about 10 μg mL^{-1}, which was a very low concentration suitable for biological applications. In addition, much less cytotoxicity was found for MSNP-Ad+ZnPc+CD-2NH_2 without the light irradiation at this concentration (Figure 3a). The MTT assay on HeLa cells without the nanoparticle addition was also carried out after exposure to 675 nm light, and no cell death was observed (Figure S12 in the SI).

The cell apoptosis pathway was investigated by flow cytometry using a moderate concentration (20 μg mL^{-1}) of MSNP-Ad+ZnPc +CD-2NH_2 (Figure 3b). A cell apoptosis/death staining kit was used, in which green fluorescence dye-conjugated annexin V binds to apoptotic cells and red fluorescence dye propidium iodide effectively stains the nucleus of dead cells. For HeLa cells treated with MSNP-Ad+ZnPc+CD-2NH_2 kept in the dark (Figure 3b-2), only a few apoptotic cells (2.07%) were detected, showing almost the same cell distribution to the control group without any treatment (Figure 3b-1). The observation indicates low cytotoxicity of the MSNP-Ad+ZnPc+CD-2NH_2 hybrid. In contrast, the treatment with the hybrid under light irradiation led to obvious cell apoptosis (Figure 3b-3). In this case, the cell population of 26.43% with high fluorescence intensity from both annexin V and propidium iodide could be attributed to dead cells that experienced the apoptosis process and were stained with both dyes, while 12.87% cells only stained with annexin V were undergoing the apoptosis process. The apoptosis/cell death analysis was also investigated by fluorescence images (Figure S13 in the SI). After the PDT treatment, considerable green dots indicating apoptotic cells and red dots indicating dead cells were observed. After merging green and red images, the individual green dots could be assigned to the apoptotic cells, while the resulting yellow dots indicate dead cells that experienced the apoptosis and cell death process.

Then, we directly compared the PDT efficacy of the MSNP-Ad+ZnPc+CD-2NH_2 hybrid with free ZnPc in solution. To fully suspend ZnPc molecules, we used a H_2O:DMSO (9:1) mixture solution for the MTT cytotoxicity assay. A certain amount of ZnPc could enter into HeLa cells, leading to a low cytotoxicity (curves 1 and 2 in Figure S14, SI). However, no detectable photodynamic cytotoxicity was observed from free ZnPc in the cells after light irradiation (curve 3 in Figure S14, SI). Interestingly, for the same amount of ZnPc in the MSNP-Ad+ZnPc+CD-2NH_2 hybrid used, effective apoptosis was observed after light irradiation (curve 4 in Figure S14, SI), indicating high PDT efficiency of the hybrid. Hence, it can be concluded that the MSNP-Ad+ZnPc+CD-2NH_2 hybrid provides effective $^1O_2$ generation and obvious cytotoxicity dependent on the concentration and light irradiation, inducing the apoptosis and death of the cancer cells.

We further investigated the biological process of photodynamic activity in MSNP-Ad+ZnPc+CD-2NH_2-induced cell apoptosis using a fluorescence microscope and Bio-TEM analysis. Intracellular localization and accumulation of the hybrid were visualized by monitoring red fluorescence from loaded ZnPc. Figure 4 shows fluorescent microscopic images of

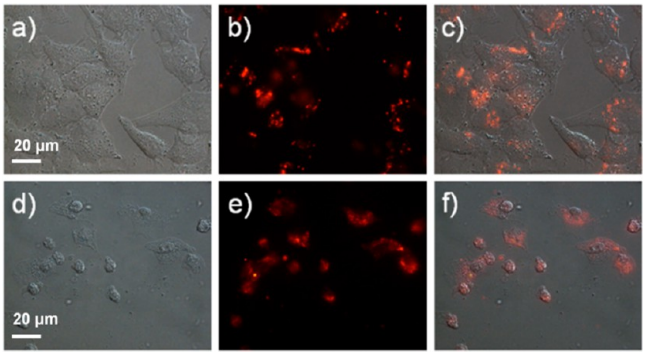

Figure 4. (a–f) Fluorescence microscopic images of HeLa cancer cells treated with MSNP-Ad+ZnPc+CD-2NH_2 (20 μg mL^{-1}). Images (a–c) are before light irradiation and (d–f) after irradiation showing completely damaged cells.

HeLa cells (60 × oil objective) treated with the hybrid for 24 h. Figures 4a–c are the images of cell lines kept in the dark. The overlay image (Figure 4c) indicates the enhanced internalization of the hybrid. Figures 4d–f are the images of cell lines incubated with the hybrid for 24 h followed by exposure to light at 675 nm for 30 min. After the irradiation, the cells were incubated for another 24 h before the observation. The morphology of HeLa cells significantly changed after the irradiation, which demonstrates that MSNP-Ad+ZnPc+CD-2NH_2 could bring serious photodynamic damage to cells for eventual apoptosis. When the cells without any treatment were irradiated by light under the same conditions, no detectable damage was observed.

Simultaneously, we conducted Bio-TEM analysis on ultrathin sections of HeLa cells treated with MSNP-Ad+ZnPc+CD-2NH_2 before and after the irradiation, to illustrate the possible uptake and localization mechanism of the hybrid. Figures 5a,b show the precise distribution of the hybrid within cells, indicating that those endocytosed hybrid-based vesicles with ellipsoidal morphology primarily accumulated in the cytoplasm. At 12 h

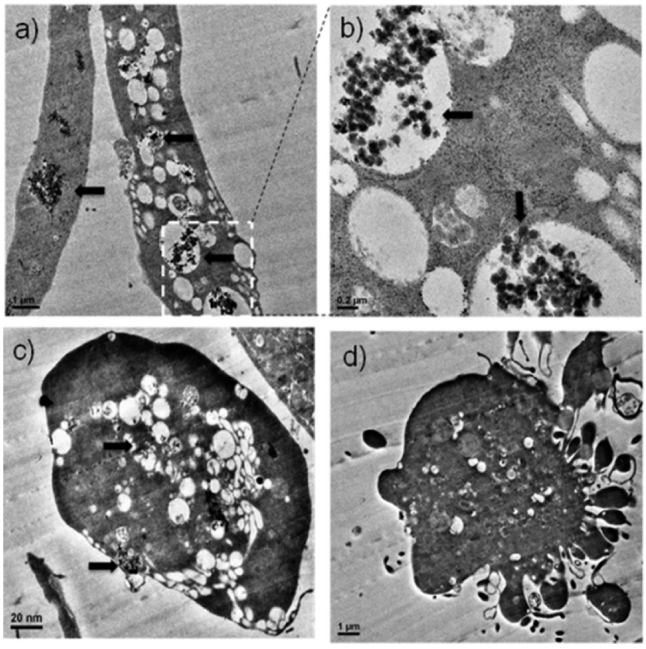

Figure 5. (a–d) Bio-TEM images of HeLa cancer cells treated with the MSNP-Ad+ZnPc+CD-2NH_2 hybrid (20 μg mL^{-1}) showing three different stages of cellular apoptosis. (a) Image showing endosome formation by the uptake of the hybrid in HeLa cells. (b) Magnified image of the section in image (a). The arrows indicate the hybrid inside the endosome of cells. (c) Morphology of cells at 12 h after the light irradiation, showing cytoplasmic shrinkage and cellular vacuolation. (d) Cells at 24 h after the irradiation displaying apoptotic bodies and membrane blebbing.

after the light irradiation, cells showed cytoplasmic shrinkage and cellular vacuolation (Figure 5c). Completely dead cell morphology was observed at 24 h after the irradiation, which displayed apoptotic bodies and membrane blebbing (Figure 5d). The experiment results confirmed that the photodynamic effect of the hybrid under the defined conditions could be employed for efficient cancer treatment.

To achieve target PDT therapy, we further modified the hybrid with FA that is widely used as a targeting ligand in cancer therapy.[46,47] As the FA receptor is usually overexpressed in most cancer cells while having a low expression in normal cells, FA receptor mediated endocytosis is expected from the FA conjugated hybrid, i.e., MSNP-Ad+ZnPc+CD-FA. After the FA conjugation, the monomeric state of ZnPc within MSNP-Ad still remained since its absorption peak at 674 nm was observed in the UV–vis spectrum of MSNP-Ad+ZnPc+CD-FA (Figure S15a in the SI). Meanwhile, a new peak around 280 nm corresponding to the FA unit proved successful conjugation of FA onto the hybrid (Figure S15a in the SI). The $^1O_2$ generation capability of MSNP-Ad+ZnPc+CD-FA was confirmed by using ADMA under a method similar to that mentioned above (Figure S15b in the SI). In this study, the HEK293 cell line was used as a normal cell model since it has a low FA receptor expression, and HeLa cells with a high FA receptor expression were employed as a cancer cell model.[46,47] Through flow cytometry analysis, we found that the FITC-labeled MSNP-Ad+ZnPc+CD-FA, i.e., MSNP(FITC)-Ad+ZnPc+CD-FA, showed higher uptake in HeLa cells as compared to that in HEK293 cells (Figure S16a in the SI). Much higher photodynamic cytotoxicity to HeLa cells was observed when they were treated with MSNP-Ad+ZnPc +CD-FA followed by light irradiation under the same conditions (Figure S16b in the SI), indicating promising application potential of MSNP-Ad+ZnPc+CD-FA towards targeted PDT therapy in the cancer treatment.

4. CONCLUSIONS

In conclusion, we have developed a novel strategy to prevent the aggregation of zinc(II) phthalocyanine (ZnPc) by loading it into the nanochannels of adamantane-functionalized mesoporous silica nanoparticles. ZnPc existed in its monomeric state inside the nanochannels and shows highly efficient singlet oxygen generation in aqueous environment upon light irradiation. Owing to the complexation of amino-substituted β-cyclodextrin with the adamantane unit on the nanoparticle surface, the ZnPc-loaded nanoparticle hybrid exhibits remarkable stability in aqueous solution and low cytotoxicity in the dark. Significant photodynamic damage to cancer cells has been achieved using the ZnPc-loaded hybrid under suitable light irradiation. This novel hybrid may serve as a promising platform for developing the next generation of photodynamic therapeutics towards specific cancer treatment.

■ ASSOCIATED CONTENT

Ⓢ Supporting Information

Characterization data of various nanoparticles, fluorescence microscopy images, cytotoxicity assay, and flow cytometry analysis. This material is available free of charge via the Internet at http://pubs.acs.org.

■ AUTHOR INFORMATION

Corresponding Author

*E-mail: zhaoyanli@ntu.edu.sg.

Author Contributions

§X.M. and S.S. contributed equally to this work.

Notes

The authors declare no competing financial interest.

■ ACKNOWLEDGMENTS

This work was financially supported by the Singapore National Research Foundation Fellowship (NRF2009NRF-RF001-015), the Singapore National Research Foundation CREATE program – Singapore Peking University Research Centre for a Sustainable Low-Carbon Future, and the NTU-A*Star Centre of Excellence for Silicon Technologies (A*Star SERC No.: 112 351 0003).

■ REFERENCES

(1) Nann, T. *Nano Biomed. Eng.* **2011**, *3*, 137–143.
(2) Bechet, D.; Couleaud, P.; Frochot, C.; Viriot, M. L.; Guillemin, F.; Barberi-Heyob, M. *Trends Biotechnol.* **2008**, *26*, 612–21.
(3) Dougherty, H.; Gomer, C. J.; Jori, G.; Kessel, D.; Korbleik, M.; Moan, J.; Peng, Q. *J. Natl. Cancer Inst.* **1998**, *90*, 889–905.
(4) Brown, S. B.; Brown, E.; Walker, I. *Lancet Oncol.* **2004**, *5*, 497–508.
(5) Celli, J. P.; Spring, B. Q.; Rizvi, I.; Evans, C. L.; Samkoe, K. S.; Verma, S.; Pogue, B. W.; Hasan, T. *Chem. Rev.* **2010**, *110*, 2795–2838.
(6) Dolmans, D. E.; Fukurma, D.; Jain, R. K. *Nat. Rev. Cancer* **2003**, *3*, 380–387.
(7) Rhodes, L. E.; de Rie, M.; Enstrom, Y.; Groves, R.; Morken, T.; Goulden, V.; Wong, G. A.; Grob, J. J.; Varma, S.; Wolf, P. *Arch. Dermatol.* **2004**, *140*, 17–23.
(8) Kato, H. *J. Photochem. Photobiol. B* **1998**, *42*, 96–99.
(9) Skyrme, R. J.; French, A. J.; Datta, S. N.; Allman, R.; Mason, M. D.; Mathews, P. N. *BJU Int.* **2005**, *95*, 1206–1210.
(10) Hopper, C.; Niziol, C.; Sidhu, M. *Oral Oncol.* **2004**, *40*, 372–382.

(11) Lee, S. J.; Koo, H.; Lee, D.-E.; Min, S.; Lee, S.; Chen, X.; Choi, Y.; Leary, J. F.; Park, K.; Jeong, S. Y.; Kwon, I. C.; Kim, K.; Choi, K. *Biomaterials* **2011**, *32*, 4021−4029.
(12) Reddi, E.; Zhou, C.; Biolo, R.; Menegaldo, E.; Jori, G. *Br. J. Cancer* **1990**, *61*, 407−411.
(13) Derycke, A.; de Witte, P. *Adv. Drug Delivery Rev.* **2004**, *56*, 17−30.
(14) Zhao, B. Z.; Yin, J. J.; Bilski, P. J.; Chingmell, C. F.; Roberts, J. E.; He, Y. Y. *Toxicol. Appl. Pharmacol.* **2009**, *241*, 163−172.
(15) Tu, H. L.; Lin, S. Y.; Lin, H.; Hung, Y.; Lo, L. W.; Chen, Y. F.; Mou, C. Y. *Adv. Mater.* **2009**, *21*, 172−177.
(16) van Nostrum, C. F. *Adv. Drug Delivery Rev.* **2004**, *56*, 9−16.
(17) Roy, I.; Ohulchansky, T. Y.; Pudavar, H. E.; Berbey, E. J.; Oseroff, A. R.; Morgan, J.; Dougherty, T. J.; Prasad, P. N. *J. Am. Chem. Soc.* **2003**, *125*, 7860−7865.
(18) Popat, A.; Hartono, S. B.; Stahr, F.; Liu, J.; Qiao, S. Z.; Lu, G. Q. *Nanoscale* **2011**, *3*, 2801−2818.
(19) Manzano, M.; Valet Regí, M. *J. Mater. Chem.* **2010**, *20*, 5593−5604.
(20) Piao, Y.; Burna, A.; Kims, J.; Weisner, U.; Hyeon, T. *Adv. Funct. Mater.* **2008**, *18*, 3745−3758.
(21) Wang, T.; Zhang, L.; Su, Z.; Wang, C.; Liao, Y.; Fu, Q. *ACS Appl. Mater. Interfaces* **2011**, *3*, 2479−2486.
(22) Valenstein, J. S.; Kandel, K.; Melcher, F.; Slowing, I. I.; Lin, V. S.-Y.; Trewyn, B. G. *ACS Appl. Mater. Interfaces* **2012**, *4*, 1003−1009.
(23) Li, Z. Y.; Liu, Y.; Wang, X. Q.; Liu, L. H.; Hu, J. J.; Luo, G. F.; Chen, W. H.; Rong, L.; Zhang, X. Z. *ACS Appl. Mater. Interfaces* **2013**, *5*, 7995−8001.
(24) Zhang, X.; Zhang, X.; Wang, S.; Liu, M.; Zhang, Y.; Tao, L.; Wei, Y. *ACS Appl. Mater. Interfaces* **2013**, *5*, 1943−1947.
(25) Sreejith, S.; Ma, X.; Zhao, Y. L. *J. Am. Chem. Soc.* **2012**, *134*, 17346−17349.
(26) Lin, Y.; Tsai, C.; Huang, H.; Kuo, C.; Hung, Y.; Huang, D.; Chen, Y.; Mou, C. *Chem. Mater.* **2005**, *17*, 4570−4573.
(27) Lu, C.; Hung, Y.; Hsiao, J.; Yao, M.; Chung, T.; Lin, Y.; Wu, S.; Hsu, S.; Liu, H.; Mou, C.; Yang, C.; Huang, D.; Chen, Y. *Nano Lett.* **2007**, *7*, 149−154.
(28) Ambrogio, M. W.; Thomas, C. R.; Zhao, Y. L.; Zink, J. I.; Stoddart, J. F. *Acc. Chem. Res.* **2011**, *44*, 903−913.
(29) Liong, M.; Liu, J.; Kovochich, M.; Xia, T.; Ruehm, S. G.; Nel, A. E.; Tamanoi, F.; Zink, J. I. *ACS Nano* **2008**, *2*, 889−896.
(30) He, Q.; Shi, J.; Chen, F.; Zhu, M.; Zhang, L. *Biomaterials* **2010**, *31*, 3335−3346.
(31) Yan, H.; Teh, C.; Sreejith, S.; Zhu, L.; Kwok, A.; Fang, W.; Ma, X.; Nguyen, K. T.; Korzh, V.; Zhao, Y. L. *Angew. Chem., Int. Ed.* **2012**, *51*, 8373−8377.
(32) Brannon-Peppas, L.; Blanchette, J. O. *Adv. Drug. Delivery Rev.* **2004**, *56*, 1649−1659.
(33) Cho, K. J.; Wang, X.; Nie, S. M.; Chen, Z.; Shin, D. M. *Clin. Cancer Res.* **2008**, *14*, 1310−1316.
(34) Nombona, N.; Maduray, K.; Antunes, E.; Karsten, E.; Nyokong, T. *J. Photochem. Photobiol. B* **2012**, *107*, 35−44.
(35) Fadel, M.; Kassab, K.; Fadeel, D. A. *Lasers Med. Sci.* **2010**, *2*, 283−72.
(36) Odaid, G.; Chambrier, I.; Cook, M. I.; Russell, D. A. *Angew. Chem., Int. Ed.* **2012**, *51*, 6158−6162.
(37) Zhao, Y. L.; Li, Z.; Kabeine, S.; Botros, Y. Y.; Stoddart, J. F.; Zink, J. I. *J. Am. Chem. Soc.* **2010**, *132*, 13016−13025.
(38) Ma, X.; Nguyen, K. T.; Borah, P.; Ang, C. Y.; Zhao, Y. L. *Adv. Healthcare Mater.* **2012**, *1*, 690−697.
(39) Stöber, W.; Fink, A. *J. Colloid Interface Sci.* **1968**, *26*, 62−69.
(40) Scalise, I.; Durantini, E. N. *Bioorg. Med. Chem.* **2005**, *13*, 3037−3045.
(41) Lau, J. T. F.; Lo, P.; Fong, W.; Ng, D. K. P. *J. Med. Chem.* **2012**, *55*, 5446−5454.
(42) Wang, F.; Yang, X.; Ma, L.; Huang, B.; Na, N.; E, Y.; He, D.; Ouyang, J. *J. Mater. Chem.* **2012**, *22*, 24597−24604.
(43) Tu, J.; Wang, T.; Shi, W.; Wu, G.; Tian, X.; Wang, Y.; Ge, D.; Ren, L. *Biomaterials* **2012**, *33*, 7903−7914.
(44) Ricci-Júnior, E.; Marchetti, J. M. *Int. J. Pharm.* **2006**, *310*, 187−195.
(45) Qian, H. S.; Guo, H. C.; Ho, P. C.-L.; Mahendran, R.; Zhang, Y. *Small* **2009**, *5*, 2285−2290.
(46) Zhang, Q.; Liu, F.; Nguyen, K. T.; Ma, X.; Wang, X. J.; Xing, B. G.; Zhao, Y. L. *Adv. Funct. Mater.* **2012**, *22*, 5144−5156.
(47) Morelli, C.; Maris, P.; Sisci, D.; Perrotta, E.; Brunelli, E.; Perrotta, I.; Panno, M. L.; Tagarelli, A.; Versace, C.; Casula, M. F.; Testa, F.; Andò, S.; Nagy, J. B.; Pasqua, L. *Nanoscale* **2011**, *3*, 3198−3207.